15. D. V. Tsivlin, V. S. Stepanyuk, W. Hergert, J. Kirschner, *Phys. Rev. B* **68**, 205411 (2003).
16. V. S. Stepanyuk *et al.*, *Phys. Rev. B* **68**, 205410 (2003).
17. Video clips and additional data are available on *Science* Online.
18. Although we know of no mention in the published literature, we believe D. M. Eigler was the first to use the tunnel current for audio feedback during atom manipulation.
19. We measured the time dependence of I at the hcp site as a function of V at fixed Z, and as a function of Z at fixed V, during atom manipulation. These two measurements are interrelated through the tunnel junction relation (and elucidate different aspects of the switching dynamics), where, at low voltages, $I = V/R$, at fixed Z, and $I = A \exp(-2\kappa Z)$, for fixed V; here, κ is the tunneling barrier decay constant. See (*29*).
20. Sh. Kogan, in *Electronic Noise and Fluctuations in Solids* (Cambridge Univ. Press, Cambridge, 1996).
21. M. B. Weissman, *Rev. Mod. Phys.* **60**, 537 (1988).
22. Errors reported in this article represent two standard deviations of the statistical uncertainty in the measurement.
23. B. N. J. Persson, *Phys. Rev. B* **44**, 3277 (1991).
24. A. J. Heinrich, C. P. Lutz, J. A. Gupta, D. M. Eigler, *Science* **298**, 1381 (2002).
25. J. Repp, G. Meyer, K.-H. Rieder, P. Hyldgaard, *Phys. Rev. Lett.* **91**, 206102 (2003).
26. L. D. Landau, E. M. Liftshitz, in *Quantum Mechanics* (Pergamon, New York, ed. 3, 1977).
27. We take the effective distance to be half the fcc-hcp distance for a constant barrier approximation that would yield the same WKB barrier integral.
28. Y. Wada, *Optoelectronics Devices Technol.* **10**, 205 (1995).
29. J. A. Stroscio, W. J. Kaiser, Eds., *Scanning Tunneling Microscopy*, vol. 27 of *Methods of Experimental Physics* (Academic Press, Boston, 1993).
30. We thank A. Fein and S. Blankenship for their assistance, and W. Gadzuk, M. Stiles, and N. Zimmerman for very fruitful discussions. Supported in part by the Office of Naval Research.

Supporting Online Material
www.sciencemag.org/cgi/content/full/1102370/DC1
Figs. S1 to S4
Movies S1 and S2

6 July 2004; accepted 25 August 2004
Published online 9 September 2004;
10.1126/science.1102370
Include this information when citing this paper.

Rescue of Cardiac Defects in *Id* Knockout Embryos by Injection of Embryonic Stem Cells

Diego Fraidenraich,[1] Elizabeth Stillwell,[1] Elizabeth Romero,[1] David Wilkes,[3] Katia Manova,[2] Craig T. Basson,[3] Robert Benezra[1]*

We report that Id knockout mouse embryos display multiple cardiac defects, but mid-gestation lethality is rescued by the injection of 15 wild-type embryonic stem (ES) cells into mutant blastocysts. Myocardial markers altered in Id mutant cells are restored to normal throughout the chimeric myocardium. Intraperitoneal injection of ES cells into female mice before conception also partially rescues the cardiac phenotype with no incorporation of ES cells. Insulin-like growth factor 1, a long-range secreted factor, in combination with WNT5a, a locally secreted factor, likely account for complete reversion of the cardiac phenotype. Thus, ES cells have the potential to reverse congenital defects through Id-dependent local and long-range effects in a mammalian embryo.

The Id proteins are dominant negative antagonists of basic helix-loop-helix (bHLH) transcription factors and regulate differentiation in multiple lineages (*1*). Previous studies have shown that Id1 to Id4 are expressed in embryonic tissues during development in partially overlapping patterns (*2*) and that Id1 and Id3 are detected at mid-gastrulation in the three germ layers (*3*). In the developing heart, Id1 to Id3 are detected in the endocardial cushion (EC) mesenchyme from embryonic day 10.5 (E10.5) through E16.5 (*2*), but Id4 is absent (*2*). Here, we show that Id1 to Id3 are also expressed in the epicardium and endocardium but are absent in the myocardium [fig. S1, A to C, for Id1; fig. S1, D and E, for Id3; (*4*) for Id2]. Id1 to Id3 expression becomes confined to the leaflets of the cardiac valves as the atrioventricular (AV) EC tissue myocardializes (*4*). Id1 and Id3 expression persists in the cardiac valves, endocardium, endothelium, and epicardium at postnatal day 7 (P7) (*4*).

Double– and triple–*Id* knockout embryos display severe cardiac defects and die at mid-gestation. *Id1*, *Id2*, or *Id3* knockout (KO) embryos do not exhibit developmental abnormalities, but ablation of two Id genes in any combination (*Id1/Id2*, *Id2/Id3*, or *Id1/Id3*) leads to embryonic lethality by E13.5 (table S1). *Id1/Id3* KO embryos display a collapse of brain vasculature with associated hemorrhage and enhanced expression of p16 and bHLH neural factors in the neighboring neuroepithelium by E12 or E13 (*5*). We wanted to identify the cause of embryonic lethality common to all KO embryos. Embryos lacking four or five copies of *Id1*, *Id2*, and *Id3* displayed multiple cardiac abnormalities at E11.5 to E13.5 (Fig. 1, A, B, D, E, G, H, J, K, M, and N for $Id1^{-/-}Id3^{-/-}$; fig. S2C for $Id1^{-/-}Id2^{-/-}$; fig. S2D for $Id1^{-/-}Id2^{+/-}Id3^{-/-}$; and fig. S2F for $Id1^{+/-}Id2^{+/-}Id3^{-/-}$). Embryo size was reduced by 10 to 30%. KO embryos displayed ventricular septal defects (VSDs) associated with impaired ventricular trabeculation and thinning of the compact myocardium. Trabeculae had disorganized sheets of myocytes surrounded by discontinuous endocardial cell lining. Cell proliferation in the myocardial wall was defective [percentage 5-bromo-2′-deoxyuridine (BrdU) ± SD: wild type (WT): 38 ± 4%; $Id1^{-/-}Id3^{-/-}$: 23 ± 3%; (Fig. 1, J to L and L inset)]. Outflow tract (OT) atresia was apparent (Fig. 1, M and N). OT and AV ECs displayed low cellularity at E11.5, which resulted in hypoplastic ECs in $Id1^{+/-}Id2^{+/-}Id3^{-/-}$ embryos at E13.5 (fig. S2, E and F). The epicardium appeared normal, and EC apoptosis was unaffected [terminal deoxynucleotidyl transferase–mediated deoxyuridine triphosphate nick end labeling (*4*)]. The impaired development of the myocardium in Id KO animals even though Ids are not expressed there suggests that Ids might participate in molecular signaling between myocardium and the Id^+ epicardium, endocardium, and EC. Alternatively, loss of Id expression in early myocardial precursors might lead to myocardial defects.

Id1/Id2/Id3 KOs have severe cardiac malformation as early as E9.5 (fig. S2, A and B). The overall size of the embryo and heart was reduced by 40 to 60%. The atrium did not separate from the ventricle, and ventricular trabeculation was rudimentary (fig. S2, A and B). No hemorrhage was observed in *Id1/Id2/Id3* KO brains at E9.5 (*4*). No triple-KO embryos survived to E11.5 (table S1). These observations suggest that a defective heart is the primary cause of mid-gestation lethality.

Injection of ES cells into Id KO blastocysts corrects cardiac defects and rescues embryonic lethality. Cardiac defects and embryonic lethality was reversed by injecting 15 β-galactosidase (*LacZ*)–marked ES Rosa 26 (R26) cells into *Id* KO blastocysts. In the resultant embryos, LacZ-positive cells were detected in the heart and forebrain (Fig. 1C). At E11.5, all cardiac structures in rescued embryos were identical to those of WT embryos. No endocardial, myocardial, or EC defects were observed (Fig. 1, C, F, I, L, and O) (*4*), and cell proliferation was restored [percentage BrdU in compact myo-

[1]Cancer Biology and Genetics Program, [2]Molecular Cytology Core Facility, Memorial Sloan-Kettering Cancer Center, [3]Molecular Cardiology Laboratory, Greenberg Cardiology Division, Department of Medicine, Weill Medical College of Cornell University, New York, NY 10021, USA.

*To whom correspondence should be addressed. E-mail: r-benezra@ski.mskcc.org

cardium: 34 ± 4% (Fig. 1L, inset)]. We determined that 25% of the litter of *Id1*$^{-/-}$ *Id3*$^{+/-}$ (or *Id1*$^{-/-}$*Id2*$^{+/-}$) or 43.75% of the litter of *Id1*$^{-/-}$*Id2*$^{+/-}$*Id3*$^{+/-}$ intercrosses should carry a null mutation in at least two Id genes, but double KOs never survive past E13.5 (table S1). However, 15 out of 75 animals (20%) of the litter of *Id1*$^{-/-}$*Id3*$^{+/-}$ and *Id1*$^{-/-}$*Id2*$^{+/-}$*Id3*$^{+/-}$ intercrosses with ES cell injection into blastocysts carried the genotype *Id1*$^{-/-}$*Id3*$^{-/-}$*:R26*, *Id1*$^{-/-}$*Id2*$^{-/-}$*:R26*, *Id1*$^{-/-}$*Id2*$^{+/-}$*Id3*$^{-/-}$*:R26*, or *Id1*$^{-/-}$*Id2*$^{-/-}$*Id3*$^{+/-}$*:R26* past E13.5 (1 out of 6 at E14.5, 5 out of 25 at E17.5, and 9 out of 45 after birth). The appearance of double-KO animals is therefore due to the presence of ES cells ($P < 0.0001$).

Rescued hearts were structurally and functionally indistinguishable from those of WT embryos by histology and echocardiography (Fig. 1, P to Z_2, and table S2). The chamber walls, septum, OT, and valves were normal (Fig. 1, P to Z_2) (*4*). Unlike *Id1/Id3* KO embryos, a continuous lining of endocardial cells apposed the myocardium in rescued pups, despite most endocardial cells not being ES-cell derived (Fig. 1, Z_1 and Z_2). In rescued pups, body and heart sizes were severely reduced during the first 3 weeks, in some cases by 50 to 70% [P15 WT, 8.33 g and 65 mg of body and heart weights, respectively; P15 *Id1*$^{-/-}$*Id3*$^{-/-}$*:R26*, 3.11 g (63% reduction) and 25 mg (62% reduction) of body and heart weights, respectively], and 44% of the rescued pups died during the first 4 weeks. The surviving rescued adult animals (5 out of 9) displayed correction of these parameters (10 to 30% reduction relative to that of WT animals by 5 to 6 weeks) (Fig. 1, X and Y). The heart/body weight ratio in WT or rescued animals was constant [heart/body ratio (±SD): $7.9 \times 10^{-3} \pm 0.5 \times 10^{-3}$], and all organs were small and grossly normal (*4*).

The average fraction of WT LacZ^{+} cells per heart was 20% (range of incorporation: 5 to 45%) and blue cells were grouped in clusters (Fig. 1, Q, U, W, and Y). The percentage of ES cell incorporation [in X-galactosidase (X-Gal) staining of tail sections] was confirmed by Southern analysis from adjacent tissue (fig. S3A). An E14.5 *Id1*$^{-/-}$*Id3*$^{-/-}$*:R26* rescued embryo with 15 ± 5% of X-Gal–positive cells displayed a WT band 80% less intense than the mutant band (Southern, fig. S3A). To rule out that X-Gal–negative cells are ES-derived cells which had lost their ability to express LacZ, individual X-Gal–negative cells were laser-captured from heart sections of an E17.5 *Id1*$^{-/-}$*Id2*$^{-/-}$*:R26* rescued embryo and shown to be *Id2*$^{-/-}$ (fig. S3B). R26 E17.5 heterozygous embryos stained uniformly blue after X-Gal staining, indicating that the result was not due to incomplete staining (Fig. 1P, inset).

In rescued hearts, a small subset of R26 cells from the epicardium, endocardium, and EC was the source of Id1/Id3 expression (fig. S1, H to J and M) (*4*). R26 cells also populated the myocardium (fig. S1, K and L), but no Ids were detected (fig. S1M) (*4*). Although it is likely that the rescue by ES cells is Id dependent, it is formally possible that ES cells incorporated into the heart provide Id-independent signals. To test this, ES cells with reduced Id1 levels by small interfering (siRNA) knockdown (fig. S3C) were injected into Id KO blastocysts. Id1 knockdown ES cells incorporated in the embryos (fig. S3D), but failed to rescue *Id1*$^{-/-}$*Id3*$^{-/-}$ blastocysts (fig. S1E).

Gene expression profiles in *Id* KO hearts are altered. Microarray analysis of E11.5 WT and *Id1/Id3* double-KO hearts (table S3) showed skeletal myosin alkali light chain (*6*) (skMLC) up-regulated 2.83-fold in mutant hearts. The enhanced signal was confirmed by Northern analysis (+2.9-fold) (Fig. 2E, inset) and ISH (Fig. 2, E and F) (*4*). Cardiac α-myosin heavy chain (α-MHC), the adult isoform, was up-regulated (+2.0-fold) (table S3). No other sarcomeric isoform was misregulated in Id-defective hearts (table S3). A switch to a complete skeletal muscle program does not occur, because the myotome-specific

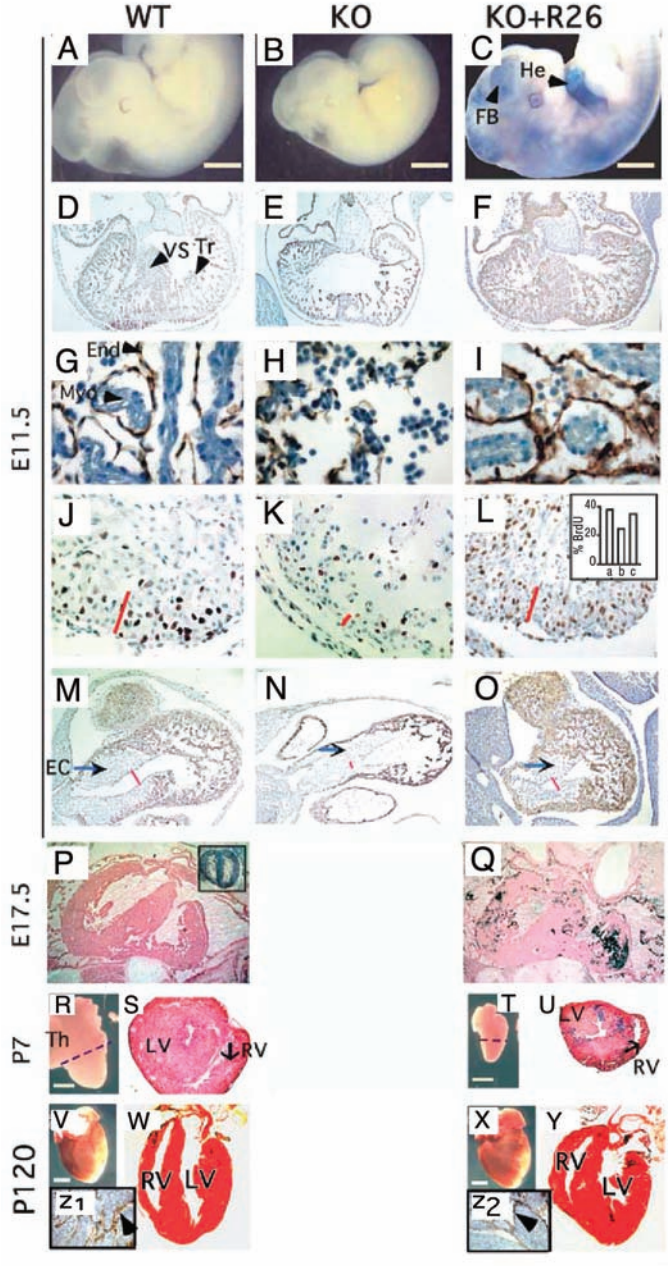

Fig. 1. Cardiac defects in *Id* KO embryos are rescued by injection of 15 ES cells. [(A) to (O)] A WT (**A**, **D**, **G**, **J**, and **M**), *Id1*$^{-/-}$*Id3*$^{-/-}$ (**B**, **E**, **H**, **K**, and **N**), or *Id1*$^{-/-}$*Id3*$^{-/-}$*:R26* (**C**, **F**, **I**, **L**, and **O**) E11.5 embryo was X-Gal stained [(A) to (C)] or transversely sectioned at the ventricle [(D) to (L)] or OT level [(M) to (O)]. (D) to (F) are magnified by 50× and (M) to (O) are magnified by 80×, desmin immunodetection. (G) to (I) show CD31 immunodetection at 200×. (J) to (L) show BrdU immunodetection at 100×. The inset in (L) shows the percentage of BrdU from (J) to (L). [(P) and (Q)] A WT (**P**), *ROSA*$^{+/-}$ [(P), inset], or *Id1*$^{-/-}$*Id3*$^{-/-}$*:R26* (**Q**) E17.5 embryo was X-Gal and eosin stained (magnified by 50×). [(R) to (Z_2)] A WT (**R** and **S**), WT:R26 (**V** and **W**), *Id1*$^{-/-}$*Id2*$^{+/-}$*Id3*$^{-/-}$*:R26* (**T** and **U**), or *Id1*$^{-/-}$*Id3*$^{-/-}$*:R26* (**X** and **Y**) P7 [(R) to (U)] or P120 [(V) to (Z_2)] heart was sectioned (dashed lines), X-Gal and eosin stained [(S) and (U), 25×; (W) and (Y), 15×) or CD31 immunostained [(Z_1) and (Z_2), 50×). He, heart; FB, forebrain; VS, ventricular septum; Tr, trabeculae; End, endocardium; Myo, myocardium; Th, thymus; LV, left ventricle; RV, right ventricle; blue arrow, outflow tract EC; KO, Id KO; red bar in (J) to (L), myocardial wall thickness; red bar in (M) to (O), luminal thickness; black arrowhead in (Z_1) and (Z_2), CD31^{+} cells. Scale bar, 500 μm [(A) to (C)]; 2 mm [(R), (T), (V), and (X)].

bHLH factors MyoD and myogenin were not detected in the *Id* KO myocardium, and α-cardiac actin was normally expressed (*4*). Stra13, a member of the Hey family of bHLH proteins (*7*, *8*) was up-regulated 4.92-fold in Id KO hearts (table S3), with enhanced Stra13 expression in the myocardium (Fig. 2, A and B). Stra13 was also detected in the neuroepithelium of the forebrain ganglionic eminence, and its expression was enhanced in the hemorrhagic *Id1/Id3* KO embryos (Fig. 2, I and J). skMLC contains E-box motifs in its enhancer (*9*). *Stra13* contains E-box motifs in the promoter and is regulated by Sharp-1, another bHLH member (*10*). α-MHC is regulated by the bHLH protein dHand. Id loss may lead to ectopic activation of bHLH proteins that in turn activate Stra13, skMLC, and α-MHC.

ES cells correct gene expression profiles in a non–cell autonomous manner. Of the misregulated markers, 82% (60 out of 74), including skMLC, α-MHC, and Stra13, were corrected in chimeric rescued hearts (table S4 and Fig. 2, C and G). The myocardium not only displayed normal skMLC or Stra13 transcript levels in R26 cells but also in *Id* KO cells (Fig. 2, C, D, G, and H). Thus, signals emanating from the R26 cells (EC, endocardium, epicardium, myocardium, or distally outside the heart) revert the myocardium in a non–cell autonomous manner.

Most of the brain endothelium was composed of *Id* KO cells (Fig. 2L). However, no collapse of the endothelium and associated hemorrhage was observed in rescued embryos (Fig. 2, K and L). Stra13 was also corrected in the neuroepithelium (Fig. 2K). Although we cannot rule out that very few R26 endothelial cells account for the rescue, a non–cell autonomous mechanism must operate because the whole of the brain endothelium appears normal.

Supernatants of epicardial cultures containing R26-derived cells rescue proliferation defects of the *Id* KO hearts. To determine whether secreted factors from *Id* KO:R26 epicardium correct proliferation defects in the *Id* KO myocardium, we derived epicardial primary cells from WT, *Id1*$^{-/-}$*Id3*$^{+/-}$, and *Id1*$^{-/-}$*Id3*$^{+/-}$*:R26* adult hearts (*11*) [reverse transcription polymerase chain reaction (RT-PCR), Fig. 3L] and collected conditioned medium (epiCM). WT and *Id1*$^{-/-}$*Id3*$^{+/-}$*:R26* but not *Id1*$^{-/-}$*Id3*$^{+/-}$ epicardial cells expressed Id1 (*4*). *Id1*$^{-/-}$*Id3*$^{+/-}$ E17.5 whole hearts were cultured for 48 hours with epiCM and BrdU and then sectioned and analyzed. WT and *Id1*$^{-/-}$*Id3*$^{+/-}$*:R26* but not *Id1*$^{-/-}$*Id3*$^{+/-}$ epiCM improved the proliferation rate of the Id KO compact myocardium relative to controls without epiCM (Fig. 3, E to H for Ki67 and insets in E to G for BrdU; compare with Fig. 3, A to D). Because *Id1*$^{-/-}$*Id3*$^{+/-}$ epiCM has little effect relative to controls with no epiCM (Fig. 3H), the R26 component of the KO:R26 epiCM (Fig. 3L, inset) accounts for the proliferation rescue. These results support the existence of an epicardial-to-myocardial rescue, through secretion of extracellular factors. We asked if misregulated myocardial markers could also be reversed. However, epiCM from WT or *Id1*$^{-/-}$*Id3*$^{+/-}$*:R26* failed to correct skMLC in E12.5 *Id1/Id3* KO hearts (Fig. 3, I to K).

Injection of ES cells into females before conception partially corrects cardiac defects and rescues embryonic lethality of the *Id* KO offspring. To investigate whether myocardial proliferation is rescued by secretion of long-range ES cell–dependent factors, 3-month-old *Id1*$^{-/-}$*Id3*$^{+/-}$ females

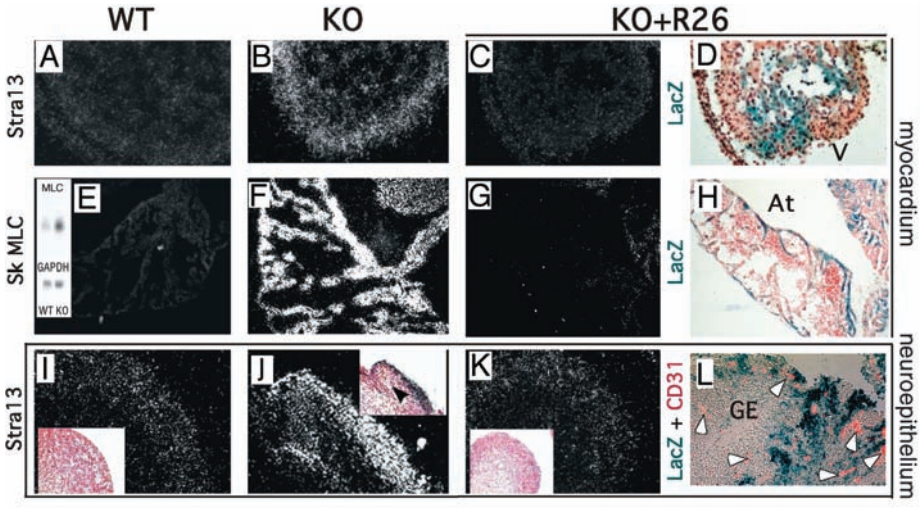

Fig. 2. R26 cells rescue *Id1*$^{-/-}$*Id3*$^{-/-}$ cells non–cell autonomously. (**A** to **C** and **I** to **K**) A WT [(A) and (I)], *Id1*$^{-/-}$*Id3*$^{-/-}$ [(B) and (J)], or *Id1*$^{-/-}$*Id3*$^{-/-}$*:R26* [(C) and (K)] E11.5 embryo was subjected to ISH for Stra13 (100×). (**D**) Adjacent section of (C), X-Gal stained. (**L**) An *Id1*$^{-/-}$*Id3*$^{-/-}$*:R26* E14.5 embryo was X-Gal and CD31 immunostained (100×). [(E) to (G)] A WT (**E**), *Id1*$^{-/-}$*Id3*$^{+/-}$ (**F**), or *Id1*$^{-/-}$*Id2*$^{+/-}$*Id3*$^{-/-}$*:R26* (**G**) P7 heart was subjected to ISH for skMLC (50×). (**H**) Adjacent section of (G), X-Gal stained. [(E), inset] Northern blot from a WT or *Id1*$^{-/-}$*Id3*$^{+/-}$ E13.5 heart probed for skMLC. Insets in (I) to (K) show bright field. V, ventricle; At, atrium; GE, ganglionic eminence; black arrowhead in (J) inset, hemorrhage; white arrowheads (L), CD31^{+} cells.

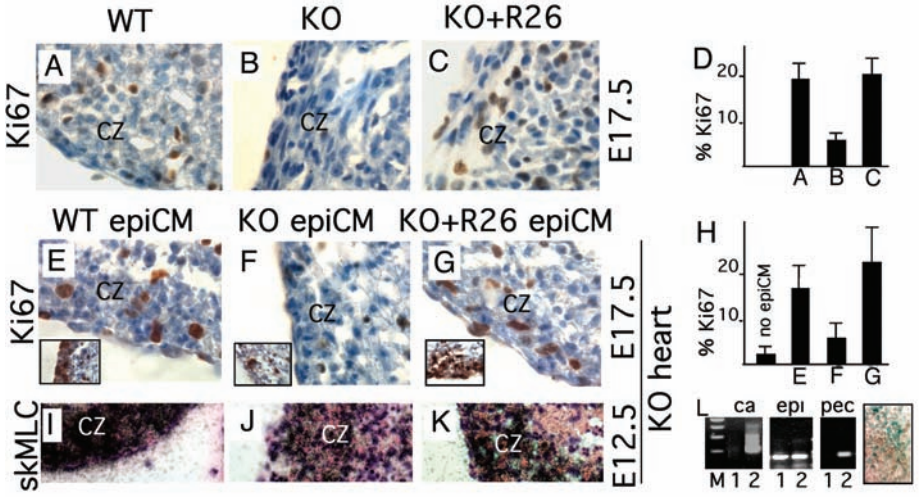

Fig. 3. Conditioned medium from *Id* KO:R26 epicardial cells (epiCM) corrects myocardial proliferation defects in *Id* KO hearts. (**A** to **C**) A WT, *Id1*$^{-/-}$*Id3*$^{+/-}$, or *Id1*$^{-/-}$*Id3*$^{+/-}$*:R26* E17.5 embryo was sectioned at heart level and Ki67 immunostained. (**D**) Percentage of Ki67^{+} cells of (A) to (C). Error bars show mean + SD. (**E** to **G** and **I** to **K**) An *Id1*$^{-/-}$*Id3*$^{+/-}$ E17.5 [(E) to (G)] or *Id1*$^{-/-}$*Id3*$^{-/-}$ E12.5 [(I) to (K)] heart was cultured with BrdU and WT [(E) and (I)], *Id1*$^{-/-}$*Id3*$^{+/-}$ [(F) and (J)], or *Id1*$^{-/-}$*Id3*$^{+/-}$*:R26* [(G) and (K)] epiCM, sectioned, and Ki67 [(E) to (G)] or BrdU [(E) to (G), insets] immunostained or subjected to ISH for skMLC [(I) to (K)]. (**H**) Percentage of Ki67^{+} cells of (E) to (G) and control with no epiCM. Error bars show mean + SD. (**L**) RT-PCR [cardiac actin (ca), epicardin (epi), and pecam (pec)] of *Id1*$^{-/-}$*Id3*$^{+/-}$*:R26* epicardial-derived cells (lane 1) or E13.5 heart (lane 2). [(L), inset] *Id1*$^{-/-}$*Id3*$^{+/-}$*:R26* epicardial-derived cells were X-Gal stained. KO, Id1$^{-/-}$Id3$^{+/-}$. Magnification: 630× in (A) to (C) and (E) to (G); 400× in (I) to (K). CZ, myocardial compact zone; M, markers.

were injected with 10^5 R26 cells intraperitoneally, and, after a week, mated with $Id1^{-/-}Id3^{+/-}$ males. Floating cells isolated from the intraperitoneal (IP) cavity and cultured formed ES cell outgrowths (fig. S3F) and embryoid bodies (*4*). R26 cells also adhered to connective tissue in the external side of the uterine wall, but no X-Gal–positive cells were detected inside the uterus or in placenta or any part of the embryo, including the yolk sac (*4*). Of newborn pups, 18% (7 out of 40) carried the $Id1^{-/-}Id3^{-/-}$ genotype, whereas no double-KO pups have been observed in over 10 years of breeding ($P < 0.001$). Double-KO pups contained no X-Gal–positive cells (Fig. 4G) (*4*) and tail DNAs were *LacZ* negative (PCR). Injection of supernatants from R26 cultures also rescued the lethality of *Id1/Id3* embryos (3 out of 35), although at lower rates (9%). The Id1/Id3 double-KO newborn pups, however, died by P2 and displayed enlarged hearts (body weight of $Id1^{-/-}Id3^{-/-}$ or WT P1 pups: 1.4 ± 0.1 g; heart weight of $Id1^{-/-}Id3^{-/-}$ P1 pups: 16 ± 1 mg; heart weight of WT P1 pups: 10 ± 1 mg; $Id1^{-/-}Id3^{-/-}$ P1 heart/body ratio: $11.4 \times 10^{-3} \pm 1.1 \times 10^{-3}$ compared with WT heart/body ratio: $7.1 \times 10^{-3} \pm 0.6 \times 10^{-3}$; $Id1^{-/-}Id3^{+/-}$:*R26* heart/body ratio at P1 was $7.3 \times 10^{-3} \pm 0.5 \times 10^{-3}$) with muscular VSDs (Fig. 4G), little endocardium, and disorganized endothelium (Fig. 4H) (compare with a WT P1 heart, Fig. 4, D and E). As with the *Id* KO hearts (with no injection), E11.5 rescued hearts (IP injection) displayed incomplete VS and discontinuous endocardium (Fig. 4, A and B). However, the thickness of the compact myocardium was corrected (Fig. 4C; compare with Fig. 1, J to L) with increased myocardial proliferation (35 ± 4% BrdU incorporation at E11.5, Fig. 4, F and I insets, for E18.5). P1 *Id1/Id3* double-KO hearts, no longer influenced by the R26 cells after birth, showed severe proliferation defects in the inner myocardium (Fig. 4, F and I).

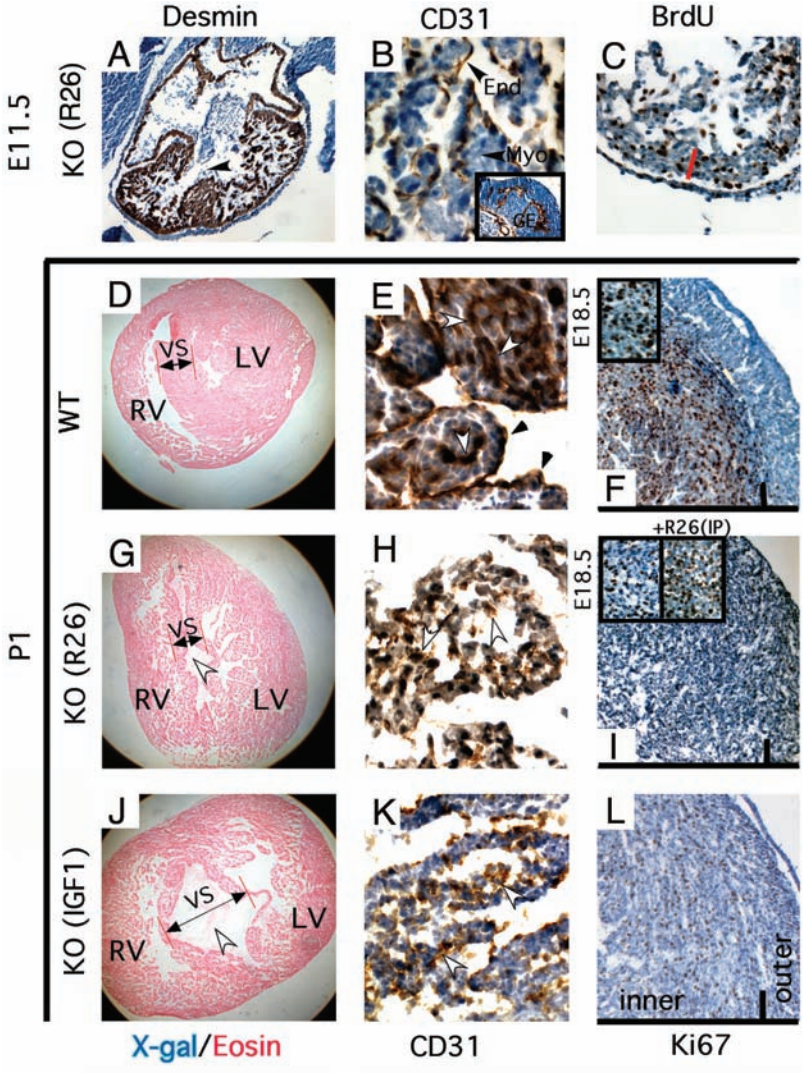

Fig. 4. *Id1/Id3* double KO pups are born from mice intraperitoneally injected with ES cells or IGF-1. (**A** to **C**) An $Id1^{-/-}Id3^{-/-}$ E11.5 embryo from an ES-injected female was sectioned at heart [(A) to (C)] or brain [(B), inset] level and Desmin [(A), 50×], CD31 [(B), 200× and (B), inset, 100×] or BrdU [(C), 100×] immunostained. [(D) to (L)] A WT (**D** to **F**), an $Id1^{-/-}Id3^{-/-}$ from an ES-injected female (**G** to **I**), or an $Id1^{-/-}Id3^{-/-}$ from an IGF-1–injected female (**J** to **L**) P1 heart was transversely sectioned and stained with X-Gal and eosin [(D), (G), and (J), 25×], CD31 [(E), (H), and (K), 200×], or Ki67 [(F), (I), and (L), 50×]. [(F) and (I), insets] A WT [(F), inset, 400×] or an $Id1^{-/-}Id3^{+/-}$ E18.5 heart from a noninjected or from an R26 injected female [(I), insets, 400×] was sectioned and Ki67 immunostained. KO(R26), Id KO embryos (pups) from R26-injected females; KO (IGF-1), *Id* KO pups from IGF-1–injected females; End, endocardium; Myo, myocardium; RV, right ventricle; LV, left ventricle; VS, ventricular septum; GE, ganglionic eminence; arrowhead (A), VS defect; red bar (C), thickness of compact myocardium; white arrowhead (G), VS defect; black arrowheads (E), $CD31^+$ endocardial cells; white arrowheads (E), $CD31^+$ endothelial cells; white arrowheads [(H) and (K)], disorganized endothelial cells.

Of the markers misregulated in *Id1/Id3* KO hearts, 64% (47 out of 74) were corrected at E11.5 after ES cell IP injection, but 36% (27 out of 74) failed to be restored (table S4). skMLC was not corrected (table S4). Mating of the same $Id1^{-/-}Id3^{+/-}$ parents without additional R26 injections rendered no double-KO pups. However, a subsequent mating with a second R26 injection led to a rescue, suggesting a reversible effect. WT murine embryonic fibroblasts (MEFs) were injected every 3 days in pregnant females, but no double-KO pups were born. Although the brain vasculature of the *Id* double-KO embryos (from IP rescue) formed an endothelial cell aggregate at E11.5 (Fig. 4B, inset), no macroscopic hemorrhage was observed.

In support of the mode of action of ES cells at a distance, $Id1^{-/-}Id3^{-/-}$:*R26* female chimeras were fertile, and when crossed with $Id1^{-/-}Id3^{+/-}$ males, 44% of the litter (4 out of 9) carried the $Id1^{-/-}Id3^{-/-}$ genotype (PCR), although these neonates died soon after birth. Thus, ES-derived cells in chimeric mothers provide distal signals during pregnancy that rescue embryonic lethality.

Identification of IGF-1 as the ES cell–secreted factor that partially corrects cardiac defects and rescues embryonic lethality of the *Id* KO offspring. To identify ES cell–secreted factors responsible for the partial cardiac rescue, we performed microarray analyses from WT, KO, or KO:R26 epicardial cultures. Because *Id* KO cultures (unlike WT or KO:R26 cultures) failed to rescue myocardial proliferation defects, we searched for secreted factors in WT or chimeric cultures with proliferation-promoting capacity, whose expression was down-regulated in *Id* KO cultures. We identified several secreted factors that showed Id-dependent regulation [table S5 (WT versus KO): IGF-1, +2; bone morphogenetic protein 4 (BMP4), –4.29; endothelin I, –3.25; table S6 (chimera versus KO): IGF-1, +1.62; BMP4, –1.52; endothelin-I, –1.62-fold). Of particular interest was IGF-1;

because it is down-regulated in *Id* KO cultures, it promotes cardiomyocyte proliferation (*12*), it is released in the bloodstream (*13*), *Id1/Id3* and *IGF-1* KO embryos are small, and Id rescued chimeras as well as *IGF-1* KO pups are small with a variable rate of postnatal lethality (*14*, *15*). IGF-1 was also down-regulated in E11.5 $Id1^{-/-}Id3^{-/-}$ hearts (–1.3-fold, according to data from microarrays).

As in the case of Ids, IGF-1 was observed at E11.5 in nonmyocardial layers of developing hearts (EC, endocardium, and epicardium) but not in the myocardium (Fig. 5, A, C, and E). IGF-1 expression was compromised in the endocardium and epicardium of $Id1^{-/-}Id3^{-/-}$ E11.5 hearts. (Fig. 5, B, D, and F). Because IGF-1 expression is not fully abrogated by Id1/Id3 loss, it is possible that Id2 sustains basal levels of IGF-1 expression. We also observed down-regulation of the 8-Kb message of IGF-1 in $Id1^{-/-}Id3^{-/-}$ E11.5 livers (Fig. 5G), the main source of circulating IGF-1. IGF-binding protein 4 (IGFBP4), an inhibitor of IGF-1 activity, was up-regulated in *Id1/Id3* KO tissues [Fig. 5G and table S5 (WT versus KO): –1.85-fold; table S7 (KO versus WT): +4.59).

We hypothesized that IGF-1 from ES cells (fig. S3G) is released into maternal circulation, passes through the placenta, and accounts for the partial rescue of $Id1^{-/-}Id3^{-/-}$ embryos. We injected IGF-1 (700 ng/day) intraperitoneally into $Id1^{-/-}Id3^{+/-}$ pregnant females, resulting in an increase in serum levels of IGF-1 (fig. S3H). Of newborn pups, 6 out of 41 (15%) carried the $Id1^{-/-}Id3^{-/-}$ genotype ($P < 0.001$). Thus, maternal injection of IGF-1 recapitulates the effect observed by maternal injection of ES cells. To test specificity of the effect and because loss of Id1 down-regulates expression of parathyroid hormone (PTH) in ES cells (*4*), we injected recombinant PTH intraperitoneally, but no *Id1/Id3* pups were born (0 out of 15). Similar to IP injection of R26 cells, pups born from IGF-1–injected mothers died by P2, and the rescued hearts were hypertrophic, with muscular VSDs and compromised endocardium and endothelium but with normal myocardial wall (Fig. 4, J to L). Thus, IGF-1 is one of the Id-dependent non–cell autonomous factors responsible for the rescue of myocardial proliferation defects.

WNT5a corrects cardiac gene expression profiles. Although maternal injection of ES cells (or IGF-1) rescues embryonic lethality and proliferation defects in *Id1/Id3* KO hearts, *Id1/Id3* KO neonates display cardiac abnormalities with altered gene expression profiles. Because the rescue in chimeric hearts generated by injection of WT ES cells in blastocysts is complete, we hypothesized that a local requirement for ES cells, which is missing in the IP rescue experiment, was critical for a full rescue. We therefore searched for locally secreted factors up-regulated in the chimeric epicardial arrays relative to *Id* KO controls. WNT5a, a noncanonical WNT, is a lipid-modified glycoprotein associated with the cell membrane and extracellular matrix (*16*) and was up-regulated 2.3-fold in chimeric versus KO as well as WT epicardial cultures (tables S5 and S6), suggesting a possible neomorphic effect of ES cells incorporated in the epicardium. Consistently, WNT5a expression was enhanced in the epicardium of E16.5 chimeric rescued hearts (fig. S4). To determine whether WNT5a corrects gene expression profiles, we performed coculture experiments in which heart explants [P1 $Id1^{-/-}Id3^{-/-}$ hearts partially rescued by maternal IP injection of R26 cells (IP R26)] were grown on MEFs overexpressing WNT5a (threefold up-regulation, according to data from microarrays). We found 653 genes misregulated between WT and *Id1/Id3* KO (IP R26) heart explants in the presence of mock-infected MEFs (table S7), including components of the WNT pathway [table S7 (KO versus WT): β-catenin, –2.64; β-catenin interacting protein, +2.3; Dkk3, –2.14-fold). Out of 653 genes, 554 (85%) were corrected when Id1/Id3 KO (IP R26) heart explants were cultured on WNT5a-overexpressing MEFs, including β-catenin, β-catenin interacting protein, and Dkk3. The adult isoform of cardiac MHC (–12.13-fold down-regulated in the Id KO explants) was corrected in the presence of WNT5a-overexpressing MEFs (table S7). It is likely that ES cells circumvent Id loss in embryonic hearts by providing WNT5a locally, which can normalize gene expression profiles.

Discussion. In this report, we demonstrate that compound *Id1/Id3* KO embryos have severe cardiac defects that result from a failure in signaling between the Id-expressing epicardium and endocardium and the Id-negative myocardium. This failure results in a thinning of the myocardial wall due to proliferation defects, VSDs, endocardial and EC defects, and OT atresia. We have been able to show that cardiac defects can be rescued by the incorporation of WT ES cells into the heart with as little as 20% chimerism. Transcriptional alterations observed in myocardial cells of *Id* KO hearts are largely restored to normal in *Id* KO cells of the chimeric hearts, indicating a non–cell autonomous rescue by WT ES cells. As in the case of Id mutant embryos, other congenital heart malformations appear to partially result from non–cell autonomous defects in cell proliferation (*17*–*19*). Although injection (aggregation) experiments with KO ES cells and WT blastocysts (morulas) have been previously reported with non–cell auton-

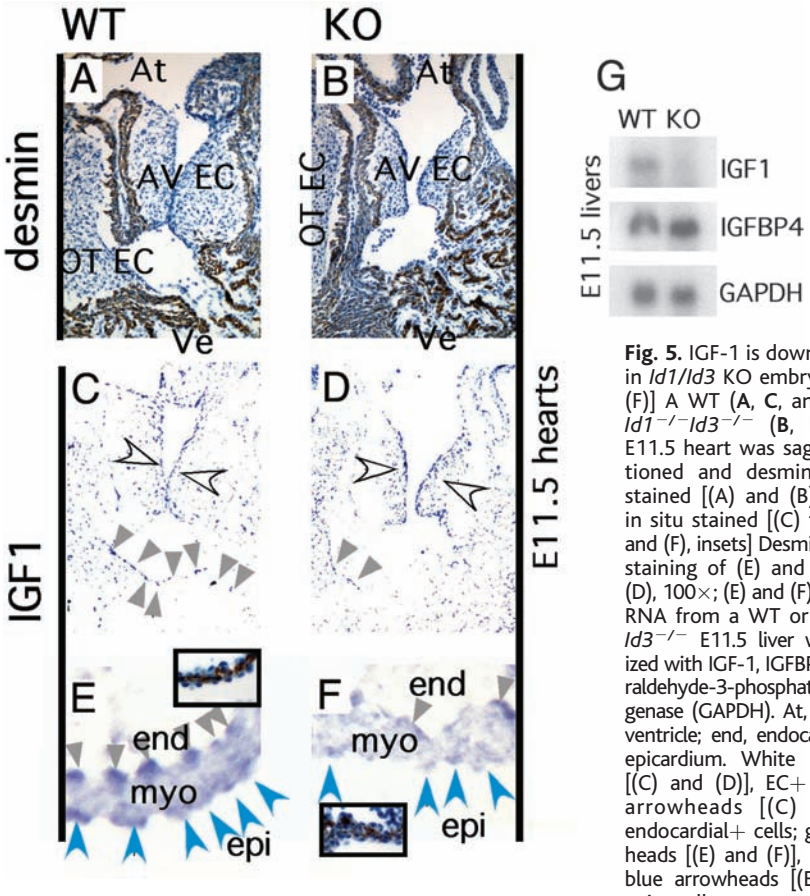

Fig. 5. IGF-1 is down-regulated in *Id1/Id3* KO embryos. [(A) to (F)] A WT (**A**, **C**, and **E**) or an $Id1^{-/-}Id3^{-/-}$ (**B**, **D**, and **F**) E11.5 heart was sagittally sectioned and desmin immunostained [(A) and (B)] or IGF-1 in situ stained [(C) to (F)]. [(E) and (F), insets] Desmin immunostaining of (E) and (F). (A) to (D), 100×; (E) and (F), 200×. (**G**) RNA from a WT or an $Id1^{-/-}Id3^{-/-}$ E11.5 liver was hybridized with IGF-1, IGFBP4, or glyceraldehyde-3-phosphate dehydrogenase (GAPDH). At, atrium; Ve, ventricle; end, endocardium; epi, epicardium. White arrowheads [(C) and (D)], EC+ cells; gray arrowheads [(C) and (D)], endocardial+ cells; gray arrowheads [(E) and (F)], end+ cells; blue arrowheads [(E) and (F)], epi+ cells.

omous correction of cardiac defects (*17*, *20*, *21*), this is the first time that low numbers of WT ES cells have been injected into blastocysts fated to die with the resultant production of viable and fertile adult animals.

The rescue we show results from a combination of long-range and short-range effects of the injected ES cells. IGF-1, secreted by ES cells, is lower in *Id* KO embryos relative to those of the WT and is restored by ES cells in chimeras or by IP injection of ES cells into mothers bearing *Id1/Id3* compound mutant embryos before conception. This latter result suggests that IGF-1 is a long-range acting factor because ES cells do not cross placenta. However, the rescue by IP injection of ES cells and direct injection of recombinant IGF-1 is incomplete with enhanced proliferation of the myocardium observed but many of the structural cardiac defects still remaining, including ventricular septal and endocardial and endothelial defects. Thus, the VS, endocardial, and endothelial defects and myocardial proliferation defects are separable, and even if VS, endocardial, and endothelial defects contribute to a defect in myocardial proliferation, this contribution can be overcome by IGF-1 administration.

Reversion of transcriptional defects of *Id* KO myocardial cells and repair of the structural defects is not achieved with IGF-1 or ES cell IP injection alone. Rather, short-range effects of ES cells incorporated into chimeric hearts are required to see this full rescue of the Id mutant heart phenotype. We have identified WNT5a, a noncanonical member of the WNT signaling family, as likely playing a key role in the rescue, given that MEFs expressing WNT5a are capable of reverting myocardial markers from KO to WT levels in 85% of the loci examined in coculture experiments. Interestingly, ES cells in chimeras are probably producing a neomorphic effect with respect to WNT5a expression because the chimeric rescued embryos have a broader WNT5a expression pattern than observed in WT embryos. Whether this broadening of WNT5a expression is required for the near complete marker reversion observed in most of the *Id* KO cells in chimeric hearts has not been demonstrated.

The ES cell rescue reported here is dependent on the expression of the Id genes, because ES cells treated with Id1 siRNA fail to effect the rescue. Interestingly, the Ids have been shown to be sufficient for self-renewal in ES cells in culture (*22*). Although the levels at which Id is required in ES cells for the cardiac rescue observed have yet to be fully elucidated, maintenance of IGF-1 expression and expansion of the WNT5a expression pattern are likely to be critical components. In any event, it is clear from these studies that ES cells can provide factors missing from mutant mammalian embryos and induce neomorphic effects that can compensate for the effects of the mutation. Such properties may imbue ES cells with a greater therapeutic value than previously imagined.

References and Notes

1. M. B. Ruzinova, R. Benezra, *Trends Cell Biol.* **13**, 410 (2003).
2. Y. Jen, K. Manova, R. Benezra, *Dev. Dyn.* **207**, 235 (1996).
3. Y. Jen, K. Manova, R. Benezra, *Dev. Dyn.* **208**, 92 (1997).
4. D. Fraidenraich *et al.*, data not shown.
5. D. Lyden *et al.*, *Nature* **401**, 670 (1999).
6. R. Kelly, S. Alonso, S. Tajbakhsh, G. Cossu, M. Buckingham, *J. Cell Biol.* **129**, 383 (1995).
7. P. Bouillet *et al.*, *Dev. Biol.* **170**, 420 (1995).
8. M. Boudjelal *et al.*, *Genes Dev.* **11**, 2052 (1997).
9. R. G. Kelly *et al.*, *Dev. Biol.* **187**, 183 (1997).
10. S. Azmi, H. Sun, A. Ozog, R. Taneja, *J. Biol. Chem.* **278**, 20098 (2003).
11. T. H. Chen *et al.*, *Dev. Biol.* **250**, 198 (2002).
12. K. Reiss *et al.*, *Proc. Natl. Acad. Sci. U.S.A.* **93**, 8630 (1996).
13. M. Adamo, W. L. Lowe, Jr., D. LeRoith, C. T. Roberts Jr., *Endocrinology* **124**, 2737 (1989).
14. L. Powell-Braxton *et al.*, *Genes Dev.* **7**, 2609 (1993).
15. J. P. Liu, J. Baker, A. S. Perkins, E. J. Robertson, A. Efstratiadis, *Cell* **75**, 59 (1993).
16. K. M. Cadigan, R. Nusse, *Genes Dev.* **11**, 3286 (1997).
17. C. M. Tran, H. M. Sucov, *Development* **125**, 1951 (1998).
18. C. J. Hatcher *et al.*, *Dev. Biol.* **230**, 177 (2001).
19. J. Chen, S. W. Kubalak, K. R. Chien, *Development* **125**, 1943 (1998).
20. H. Wu, S. H. Lee, J. Gao, X. Liu, M. L. Iruela-Arispe, *Development* **126**, 3597 (1999).
21. D. E. Clouthier, S. C. Williams, R. E. Hammer, J. A. Richardson, M. Yanagisawa, *Dev. Biol.* **261**, 506 (2003).
22. Q. L. Ying, J. Nichols, I. Chambers, A. Smith, *Cell* **115**, 281 (2003).

23. We thank J. Massague and members of the Benezra lab for critically reading the manuscript, W. Mark, J.-H. Dong (Transgenic Facility), A. Viale (Microarray Facility), S. Curelariu (technical assistance), P. Soriano (R26 cells), Y. Yokota (Id2-deficient mice), V. Mittal and S. Gupta (Id1 knockdown ES cells), and the Molecular Cytology Core Facility. D.F. and R.B are funded by NIH grants KO1HL076568-01 and R01CA107429, respectively. C.T.B. is an AHA established investigator and supported by the Snart Cardiovascular Fund.

Supporting Online Material

www.sciencemag.org/cgi/content/full/306/5694/247/DC1
Material and Methods
Figs. S1 to S4
Tables S1 to S7
References

12 July 2004; accepted 13 August 2004

REPORTS

The Structure of Catalytically Active Gold on Titania

M. S. Chen and D. W. Goodman*

The high catalytic activity of gold clusters on oxides has been attributed to structural effects (including particle thickness and shape and metal oxidation state), as well as to support effects. We have created well-ordered gold monolayers and bilayers that completely wet (cover) the oxide support, thus eliminating particle shape and direct support effects. High-resolution electron energy loss spectroscopy and carbon monoxide adsorption confirm that the gold atoms are bonded to titanium atoms. Kinetic measurements for the catalytic oxidation of carbon monoxide show that the gold bilayer structure is significantly more active (by more than an order of magnitude) than the monolayer.

Highly dispersed Au particles exhibit exceptional catalytic activity for several reactions, including CO oxidation (*1*, *2*). On the basis of kinetic studies and scanning tunneling microscopy (STM) data, the most active structures of Au have been shown to consist of bilayer islands (*2*–*4*) that have distinctive electronic (*4*) and chemical (*5*, *6*) properties compared to bulk Au. Other explanations based on the Au particle shape or perimeter (*7*), the Au-oxide contact area (*8*), the metal oxidation state (*9*), and support effects (*7*, *10*) have also been proposed to account for the special catalytic properties of nanostructured Au particles (*11*, *12*). We now report an atomic-level, structure-activity relation for the catalytic activity of supported Au. Specifically, two well-ordered Au films, a (1×1) monolayer (ML) and a (1×3) bilayer, completely wet an ultrathin titanium oxide (titania) surface that was grown on a Mo(112) surface. Unprecedented catalytic activity for CO

Department of Chemistry, Texas A&M University, College Station, TX 77842–3012, USA.

*To whom correspondence should be addressed. E-mail: goodman@mail.chem.tamu.edu